Proceedings of the LHCP2015 Conference, St. Petersburg, Russia, August 31 - September 5, 2015

Editors: V.T. Kim and D.E. Sosnov

Semileptonic (lepton, neutrino and jets) WW/WZ resonances search at $\sqrt{s} = 8$ TeV with the ATLAS detector at the LHC

EVGENIYA CHEREMUSHKINA

State Research Center of Russian Federation — Institute for High Energy Physics of National Research Center "Kurchatov Institute", 1, Nauki square, 142281, Protvino, Moscow region, Russian Federation

evgenia.cheremushkina@cern.ch

On behalf of the ATLAS Collaboration

Abstract. This poster presents the analysis results of the diboson (WW or WZ) resonances production search in pp collisions at $\sqrt{s} = 8$ TeV with the ATLAS detector at the LHC in 2012, using a total integrated luminosity of 20.3 fb^{-1}. The analysis is optimized for two benchmark signal models: Randall-Sundrum model (Spin-2 RS G^*) for WW and Extended Gauge Model (Spin-1 EGM W') for WZ resonances. The search is performed for semileptonic final state, i.e. one W boson decays to lepton (electron or muon) and neutrino and other W or Z — hadronically. No significant excess for diboson resonances production is observed and upper limits on the production cross section times branching fraction of G^* and W' are determined at 95% CL. Resonance masses below 760 GeV for G^* and 1490 GeV for W' are excluded, that gives a significant improvement to the results over previously reported limits in the same final state.

INTRODUCTION

There are several physics models, such as Supersymmetry, Technicolor, Extra Dimensions, which predict new particles, that can decay to gauge bosons pairs. This poster presents the results of the analysis, that strategy is optimized by using Randall-Sundrum (RS) model [1] and Extended Gauge Model (EGM) [2] and based on the diboson (WW for Spin-2 RS G^* or WZ for Spin-1 EGM W') resonances production search. Figure 1 shows s-channel leading-order Feynman diagrams for $G^* \to WW$ (a) and $W' \to WZ$ (b) production. The search is performed for semileptonic final state, i.e. one W boson is decayed to lepton (electron or muon) and neutrino and other W or Z — hadronically.

This analysis is made on data, collected in pp collisions at $\sqrt{s} = 8$ TeV by the ATLAS detector [3] at the LHC in 2012, using a total integrated luminosity of 20.3 fb^{-1} [4].

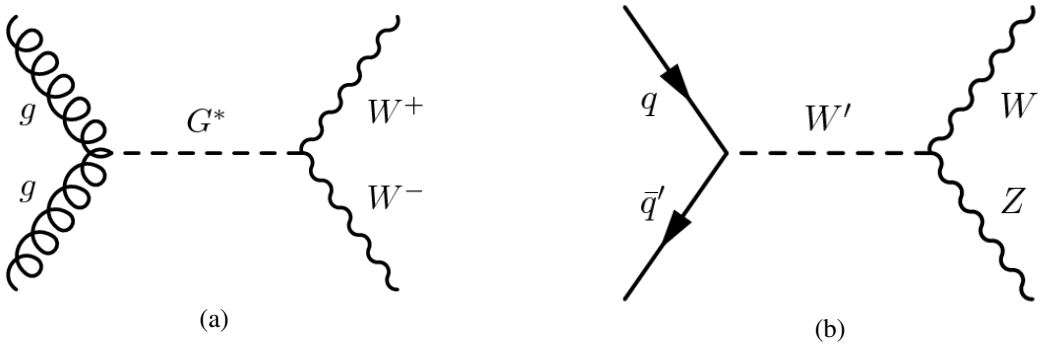

FIGURE 1. s-channel leading-order Feynman diagrams for $G^* \to WW$ (a) and $W' \to WZ$ (b) production [4].

EVENT SELECTION

In accordance with the analysis final state, interesting objects within an event are leptons (electrons or muons), jets and missing transverse momentum ($E_{\mathrm{T}}^{\mathrm{miss}}$). Each event should have at least 1 primary vertex with at least 3 associated tracks. The primary vertex is chosen with the largest sum of the tracks transverse momenta $\sum p_{\mathrm{T}}^2$. Also events are required to pass single lepton trigger.

Two different lepton categories are used for the selection procedure: "signal" — for the final analysis and "veto" — for the orthogonalization of this analysis with other final state topologies, such as *lvll*, *llqq*. Lepton candidates both electrons and muons are required to have transverse momentum $p_{\mathrm{T}} > 25$ GeV (20 GeV) and $|z_0 \sin\theta| < 0.5$ mm (2 mm) for "signal" ("veto"), where z_0 is the longitudinal impact parameter of the lepton with respect to the reconstructed primary vertex and θ — polar angle, track isolation $p_{\mathrm{T}}^{\mathrm{cone20}}/E_{\mathrm{T}} < 0.15$ for both "signal" and "veto", calorimeter isolation $E_{\mathrm{T}}^{\mathrm{cone20}}/E_{\mathrm{T}} < 0.14$ only for "signal" leptons, where $p_{\mathrm{T}}^{\mathrm{cone20}}$ ($E_{\mathrm{T}}^{\mathrm{cone20}}$) is a scalar sum of p_{T} of charged particle tracks (E_{T} in calorimeters) within a cone in η-ϕ plane (η — pseudorapidity and ϕ —azimuthal angle) of a radius $R = \sqrt{\eta^2 + \phi^2} = 0.2$ around the candidate excluding its own track (cluster). Also both "signal" and "veto" leptons should satisfy $|\eta| < 2.47$ excluding crack region $1.37 < |\eta| < 1.52$ ($|\eta| < 2.5$) and $|d_0/\sigma(d_0)| < 6$ (3.5) for electrons (muons), where d_0 is the transverse impact parameter and $\sigma(d_0)$ is the uncertainty on the measured d_0.

Tree different jet selections with three corresponding signal regions, depending on p_{T} of the leptonically (W) and hadronically (W or Z) decayed bosons, are used in the analysis. For the low-p_{T} hadronically decayed W/Z bosons, two leading jets, reconstructed by anti-k_t algorithm with $R = 0.4$ (small-R jets) are selected. This region is called Low-p_{T} Resolve Region (LLR). The small-R jets are required to pass next criteria: $p_{\mathrm{T},j} > 30$ GeV, $|\eta| < 2.8$, $p_{\mathrm{T},jj} > 100$ GeV, $p_{\mathrm{T},W\to lv} > 100$ GeV. For the high-p_{T} hadronically decayed W/Z bosons, one boosted leading jet, reconstructed by Cambridge–Aachen algorithm with $R = 1.2$ (large-R jet) is selected. This is called Merged Region (MR). The large-R jet has to be with $p_{\mathrm{T},J} > 400$ GeV, $|\eta| < 2.8$, as well as for leptonically decayed W $p_{\mathrm{T},W\to lv} > 400$ GeV. To optimize the selection in the transition area between LRR and MR High-p_{T} Resolve Region (HRR) is included with the selection: $p_{\mathrm{T},j} > 80$ GeV, $|\eta| < 2.8$, $p_{\mathrm{T},jj} > 300$ GeV, $p_{\mathrm{T},W\to lv} > 300$ GeV. Furthermore, for all three signal regions b-jet veto and invariant jet mass cut $65 < m_{jj/J} < 105$ GeV are applied. Prioritization for signal regions is done by applying firstly MR selection, events which are not passed MR then run through HRR cuts and then LRR requirements.

The missing transverse momentum is calculated as the negative of the vectorial sum of the transverse momenta of all electrons, muons, and jets, that are not associated with any other objects.

The analysis includes two channels, according to the lepton flavor. The criteria applied to select signal events are: exactly one "signal" lepton (muon or electron) and no additional "veto" leptons both flavors, $E_{\mathrm{T}}^{\mathrm{miss}} > 30$ GeV, exactly 2 small-R jets or 1 large-R jet. Figure 2 shows the signal efficiency for G^* (a) and W' (b) in both muon and electron channels and three signal regions [4].

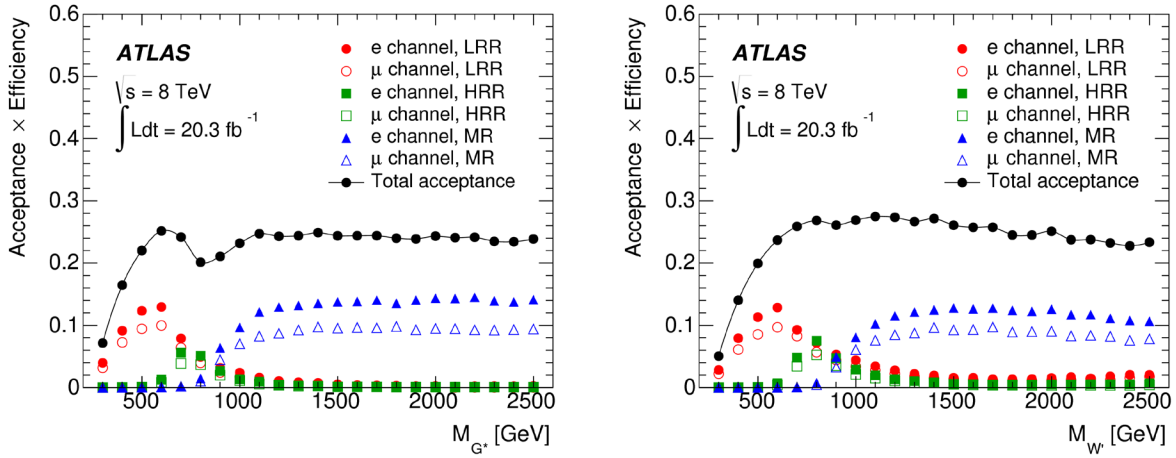

FIGURE 2. G^* (a) and W' (b) signal efficiencies in both channels and three signal regions. The efficiency is expressed with respect to the total number of $WW \to lvqq$ for G^* and $WZ \to lvqq$ for W' events with $l = e, \mu, \tau$ [4].

BACKGROUND ESTIMATION

The dominant background for this analysis arises from Standard Model (SM) production of the W/Z+jets, where one lepton from W or Z can be selected as a "signal" lepton and jets mimic hadronically decayed W or Z bosons. The backgrounds from SM production of single t and $t\bar{t}$ (top) are predominant, as a t quark decays to b quark and W boson. The next significant background appears from multijet production, that can mimic the analysis final state due to misidentification leptons. And finally, the small contribution from SM diboson production (WW, WZ, ZZ, $W\gamma$, $Z\gamma$) increases the total background.

The shapes of the W/Z+jets, top and diboson backgrounds are taken from the Monte Carlo (MC) simulation in the signal, control and validation regions. The shape of the multijet background is obtained by data driven method by creating enriched multijet data sample. The top and diboson backgrounds are normalized to the number of events from MC background samples. The normalizations of the W/Z+jets and multijet backgrounds are estimated by data driven method using the events in a control region, where the inverted cut on invariant mass is required: $45 < m_{jj/J} < 65$ GeV and $105 < m_{jj/J} < 200$ GeV. They are determined from binned minimum χ^2 fits to the $E_{\mathrm{T}}^{\mathrm{miss}}$ distributions in the control data samples corresponding to each signal region and channel separately. The fitted parameters are the normalizations of the W/Z+jets and multijet processes. Figure 3 shows an example for the low-p_{T} resolved region [4]. Multijet background is validated by the enriched multijet sample, that is obtained by inverting $E_{\mathrm{T}}^{\mathrm{miss}}$ cut: $E_{\mathrm{T}}^{\mathrm{miss}} < 30$ GeV for electron channel and $50 < E_{\mathrm{T}}^{\mathrm{miss}} < 80$ GeV for muon channel. $t\bar{t}$ background is also validated by the enriched top pairs sample by requiring at least 1 b-jet in the event.

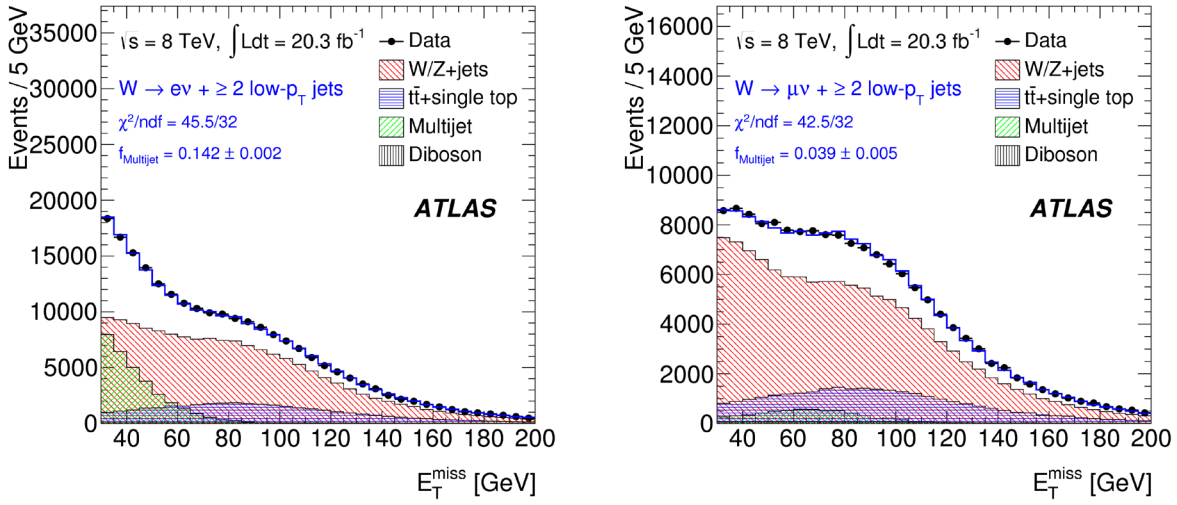

FIGURE 3. χ^2 fit to the E_T^{miss} spectrum in the electron (a) and muon (b) channels for the selected events of the W/Z+jets control sample in the low-p_T resolved regime. For reference, the fraction of the multijet background contribution ($f_{Multijet}$) is also calculated. The errors shown here are statistical only [4].

SYSTEMATIC UNCERTAINTIES

The systematic uncertainties on the background estimation, such as uncertainties on scale and shape of the W/Z+jets, multijet, $t\bar{t}$ and diboson backgrounds are included in the analysis. Also uncertainties due to single top production, parton distribution functions (PDF), initial- and final-state radiation modeling (ISR and FSR) uncertainties of the $t\bar{t}$ background are estimated. For the objects reconstruction the following sources of uncertainties are considered: for the leptons — electron and muon reconstruction, electron energy scale and resolution, muon momentum scale and resolution, for the missing transverse momentum — missing transverse momentum soft terms, for jets reconstruction — jet energy scale and resolution, jet mass scale and resolution, jet vertex fraction, momentum balance scale and resolution and b-tagging uncertainties. The dominant uncertainties on the signal come from ISR/FSR and PDF uncertainties. The uncertainty associated to the measurement of the integrated luminosity is also considered [4].

RESULTS AND INTERPRETATION

On Figure 4 (a) the table shows the total number of observed and predicted events for three signal regions and on Figure 4 (b) the histogram shows the reconstructed invariant mass m_{lvJ} distributions for data and backgrounds and also signal models in the merged signal region for the combined electron and muon channels [4]. There is a good agreement between data and background. 95% CL upper limits on the production cross section times branching fraction of RS G^* and EGM W' are determined for the interpretation of the result. These limits are calculated by performed fit of the likelihood to $m_{lvjj/J}$ by RooStats [5]. Upper limits are obtained using the CLs method [6] applied to binned histograms (templates) derived from MC. The fit is performed simultaneously to the electron and muon channels. In each channel five components are included in the fit for the $lvjj/J$ final state: signal (G^* or W'), W/Z+jets, multijet, top and diboson backgrounds. Systematic uncertainties are included as nuisance parameters. All tree signal regions and two lepton channels are combined. In order to stabilize the combined fit, not all tree signal regions are used in each mass point. A region is only used if it contributes more than 10% of the total signal sensitivity. The likelihood is performed for LRR from 300 to 800 GeV, for HRR from 600 to 1000 GeV and for MR from 800 to 2000 GeV. Figure 5 shows observed and expected 95% CL upper limits on the cross section times branching fraction as a function of the resonance pole mass for the G^* (a) and W' (b). The LO theoretical cross sections for G^* (a) and NNLO theoretical cross sections for W' (b) production are also shown. Resonance masses below 760 GeV and 1490 GeV are excluded for G^* and W' accordingly [4]. The shoulder, observed around 800 GeV, is a result of the transition between the high-p_{T} resolved and merged region.

Sample	LRR	HRR	MR
$W/Z+$jets	104800 ± 1600	415 ± 10	180 ± 20
$t\bar{t}+$single top	37700 ± 1600	271 ± 13	42 ± 7
Multijet	13500 ± 500	84 ± 9	29.3 ± 2.9
Diboson	5500 ± 270	96 ± 6	43 ± 7
Total	161500 ± 2300	870 ± 40	295 ± 22
Data	157837	801	323
G^* signal	7000 ± 500	36 ± 6	5.5 ± 2.3
W' signal	6800 ± 600	318 ± 21	70 ± 4

(a)

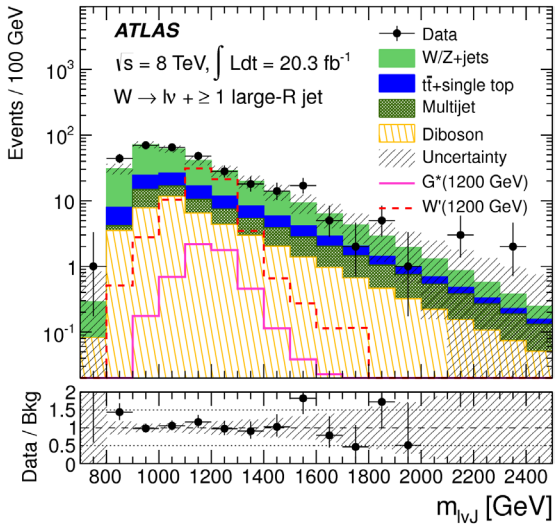

(b)

FIGURE 4. (a) the total number of observed and predicted events for tree signal regions, (b) the reconstructed m_{lvJ} distributions for data and backgrounds and also signal models in the merged signal region for the combined electron and muon channels [4].

CONCLUSION

As a result of the analysis no evidence for resonant diboson production is observed. 95% CL upper limits on the production cross section times branching fraction of G^* and W' are determined. Also resonance masses below 760 GeV and 1490 GeV are excluded for G^* and W' respectively [4], that is stricter as compared with the previous 7 TeV analysis results with lower limits on resonance masses 710 GeV for G^* and 950 GeV for W' [7]. Comparative results of other parallel 8 TeV analyses with different final states for ATLAS and CMS experiments are shown in Table 1. This analysis sets the most stringent limit for G^* resonance mass. Observed limit for the W' resonance mass is competitive with the ones obtained in parallel analyses.

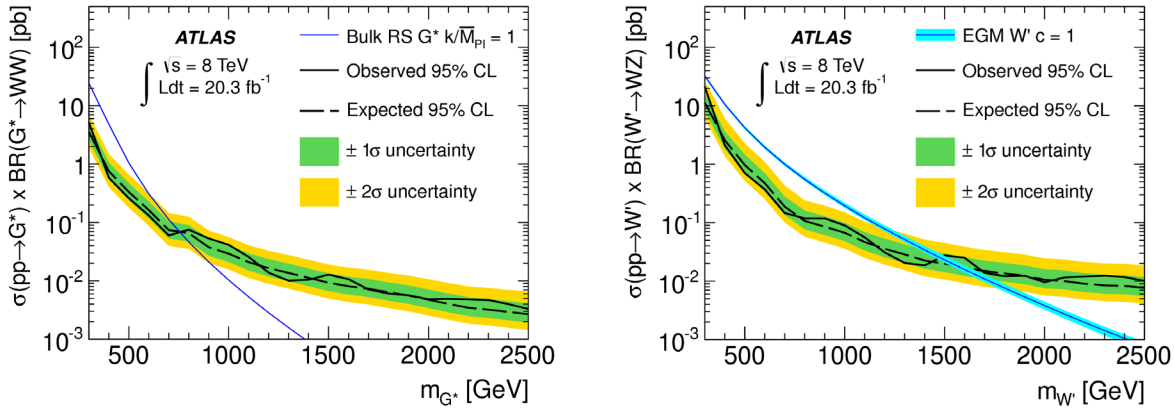

(a) (b)

FIGURE 5. Observed and expected 95% CL upper limits on the cross section times branching fraction as a function of the resonance pole mass for the G^* (a) and W' (b). The LO theoretical cross sections for the G^* (a) and NNLO theoretical cross sections for the W' (b) production are also shown. The inner and outer bands around the expected limits represent $\pm 1\sigma$ and $\pm 2\sigma$ variations respectively [4].

TABLE 1. Lower limits on resonance masses for 8 TeV analyses with semileptonic *lvqq* [4], semileptonic *llqq* [8], fully leptonic *lvll* [9] and fully hadronic *qqqq* [10] final states for ATLAS and semileptonic *lvqq* [11], fully leptonic *lvll* [12] and fully hadronic *qqqq* [13] for CMS experiments.

Experiments	**Channels**	$M(G^*)$	$M(W')$
ATLAS	$WW/WZ \to lvqq$	760 GeV	1490 GeV
	$WZ/ZZ \to llqq$	740 GeV	1590 GeV
	$WZ \to lvll$	—	1520 GeV
	$WW/WZ/ZZ \to qqqq$	2 TeV 2.6σ (WW)	1500 GeV
		2 TeV 2.9σ (ZZ)	2 TeV 2.5σ
CMS	$WW/WZ \to lvjj$	No limit set	—
	$WZ \to lvll$	—	1470 GeV
	$WW/WZ \to qqqq$	No limit set	1700 GeV

ACKNOWLEDGMENTS

This work is supported by the Russian MES grant RFMEFI61014X0005 and Presidential Grant NSh-999.2014.2 (Russia).

REFERENCES

[1] L. Randall and R. Sundrum, Phys. Rev. Lett. **83**, 3370–3373 (1999).
[2] G. Altarelli, B. Mele, and M. Ruiz-Altaba, Z. Phys. C **45**, p. 109 (1989).
[3] ATLAS Collaboration, JINST **3**, p. S08003 (2008).
[4] ATLAS Collaboration, Eur. Phys. J. C **75**, p. 370 (2015).
[5] L. Moneta and K. Belasco, PoS **ACAT2010**, p. 057 (2010).
[6] A. L. Read, J. Phys. G **28**, p. 2693 (2002).
[7] ATLAS Collaboration, Phys. Rev. D **87**, p. 112006 (2013).
[8] ATLAS Collaboration, Eur. Phys. J. C **75**, p. 69 (2015).
[9] ATLAS Collaboration, Phys. Let. B **737**, 223–243 (2014).
[10] ATLAS Collaboration, arXiv:1506.00962 [hep-ex] (2015).
[11] CMS Collaboration, JHEP **08**, p. 174 (2014).
[12] CMS Collaboration, Phys. Let. B **740**, 83–104 (2015).
[13] CMS Collaboration, JHEP **08**, p. 173 (2014).